ISSN 1063-7729, Astronomy Reports, 2016, Vol. 60, No. 12, pp. 1052–1066. © Pleiades Publishing, Ltd., 2016.
Original Russian Text © T.N. Tarasova, 2016, published in Astronomicheskii Zhurnal, 2016, Vol. 93, No. 12, pp. 1029–1044.

A Study of the Shell of Nova V2659 Cyg

T. N. Tarasova*

Crimean Astrophysical Observatory, Russian Academy of Sciences, Nauchny, Russia

Received February 9, 2016; in final form, May 5, 2016

Abstract—Results of a study of the shell of Nova V2659 Cyg based on spectrophotometric observations carried out over a year and a half after its eruption are presented. The physical conditions in the nova shell have been studied. The electron temperature (9000 K) and density (5×10^6 cm^{-3}) in the nebular stage have been estimated, together with the abundances of helium, oxygen, nitrogen, neon, argon, and iron. The abundances of nitrogen, oxygen, neon, and argon are enhanced relative to the solar values. The relative abundances are $[N/H] = 2.26 \pm 0.25$ dex, $[O/H] = 1.66 \pm 0.35$ dex, $[Ne/H] = 0.78 \pm 0.25$ dex, and $[Ar/H] = 0.32 \pm 0.38$ dex. The estimated mass of oxygen and total mass of the emitting shell are $\approx 1 \times 10^{-4}\ M_\odot$ and $\approx 3 \times 10^{-4}\ M_\odot$, respectively. In the period of chaotic brightness oscillations, the maximum velocity of the shell expansion derived from the radial velocities of the absorption components of the HI and FeII line profiles increased by ≈400 km/s 41 days after the maximum, and by ≈200 km/s 101 days after the maximum, reaching 1600 km/s in both cases.

DOI: 10.1134/S106377291611007X

1. INTRODUCTION

Nova V2659 Cyg was discovered at 31.8 UT in March 2014 [1], when its brightness was 10.9^m. After the discovery of the nova, its brightness increased, reaching about 9.3–9.4^m at its maximum. The name of the nova was assigned in [2]. The spectra obtained a day after the detection [1] showed that this was a FeII nova. Our observations cover the period from the 17th to the 569th day after the maximum. Starting from the brightness maximum up to the beginning of its smooth decline, a chaotic increase and decrease of the brightness by ≈ 1–2^m was observed. At the time of these chaotic oscillations of the brightness, the intensity and radial velocity of the absorption components of the HI and FeII lines varied. Moreover, the shape and intensity of the emission components of the line profiles also varied. We have examined how these characteristics of the line profiles changed with the brightness variations. We have also estimated some physical parameters of the nova shell based on calculations of the line fluxes when the nova shell became transparent to the radiation of the white dwarf: the electron density, abundances of some elements, and the mass of the shell.

2. OBSERVATIONS

Spectral observations were carried out by the 2.6-m Shain mirror telescope of the Crimean Astrophysical Observatory(CrAO). All the spectra were obtained with a resolution close to 1000 using the SPEM slit spectrograph installed at the Nasmyth focus. The detector was a SPEC-10 (1340 × 100 pixel) CCD camera. The dispersion for the 651 line/mm grating was about 2 Å/pix. The initial reduction of the spectra, including subtraction of the bias and correction for inhomogeneity of the CCD field sensitivity was carried out using the SPERED code, written by S. Sergeev at the CrAO. The wavelength scale of the spectraum was calibrated using the spectrum of a He–Ne lamp. The flux scale was calibrated out using the absolute spectral energy distribution of the spectrophotometric standard HR 7744, taken from [3]. This standard was observed on the same date and at the same zenith distance as V2659 Cyg. Therefore, the difference in the air masses of the standard star and the nova was not taken into account. Since we used a slit spectrograph, we compared the observed magnitudes of V2659 Cyg in the B and V filters with B and V color indices calculated from calibrated spectra obtained on the dates of our observations. If there was no information on the photometric flux of the nova for a given date, we interpolated these data from nearby dates. The difference between the calculated and measured magnitudes of the nova was, on average, about 0.1^m.

3. LIGHT CURVE AND PHOTOMETRIC CHARACTERISTICS OF THE NOVA

The light curve of Nova V2659 Cyg based on data from the AAVSO database is shown in Fig. 1,

*E-mail: taya@crao.crimea.ua

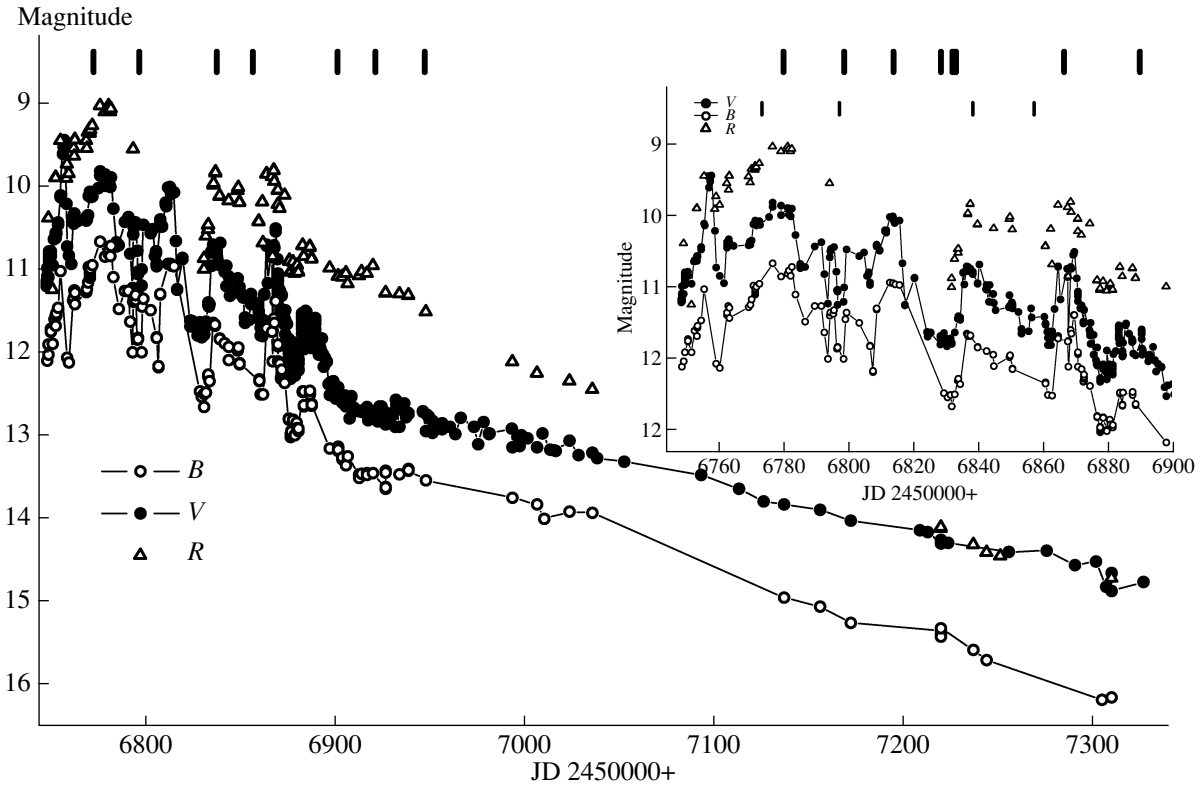

Fig. 1. Light curves of V2659 Cyg in the B (open circles), V (points), and R (triangles) filters. The data were taken from the AAVSO database. The insert shows observations with higher temporal resolution. The bars at the top of the figure show the times of the spectral observations.

which presents the B, V, and R brightness variations during our observations. The star chaotically became brighter by 1 to $\approx 2^m$ during the 140 days after the maximum brightness. A sharp brightening at the initial stage of the brightness decline was reported by Imamura et al. [4] and Chochol et al. [5]. The parameter t_2 was obtained from photometric observations in [5]. We used the AAVSO light curve shown in Fig. 1 to derive a t_2 value close to 60^d. The value of parameter t_3 is close to 150^d. It is clear that this nova is moderately fast. However, the determination of t_2 is hampered by the irregular variations in the light curve. Using this parameter, Chochol et al. [5] estimated the absolute maximum brightness of the nova to be -6.7 ± 0.04^m. They also estimated the mass of the white dwarf to be $0.65 \pm 0.02\ M_\odot$.

4. SPECTRAL EVOLUTION

Figure 2 shows all our spectrophotometric observations, and Table 1 a journal of the observations. The journal lists the observation dates and Julian dates and the number of days since the maximum brightness. The last column indicates the spectral range of the spectrum.

The vertical bars above the light curve in Fig. 1 mark the epochs of our spectroscopic observations.

Table 1. Journal of observations of V2659 Cyg

Date	JD 2450000+	Day	Spectral range, Å
27.04.14	6773.550	17	3225–7525
20.05.14	6797.449	41	3200–7575
29.06.14	6838.449	82	3200–7575
18.07.14	6857.386	101	3213–7574
01.09.14	6902.300	146	3200–7575
21.09.14	6922.300	166	3225–7575
17.10.14	6948.244	192	3200–7574
27.05.15	7169.504	413	3359–7525
22.06.15	7195.503	439	3264–7575
16.07.15	7220.494	464	3374–7525
22.07.15	7226.415	470	3343–7525
23.07.15	7227.493	471	3355–7525
24.07.15	7228.409	472	3377–7524
19.09.15	7285.405	529	3378–7524
29.10.15	7325.300	569	3676–7524

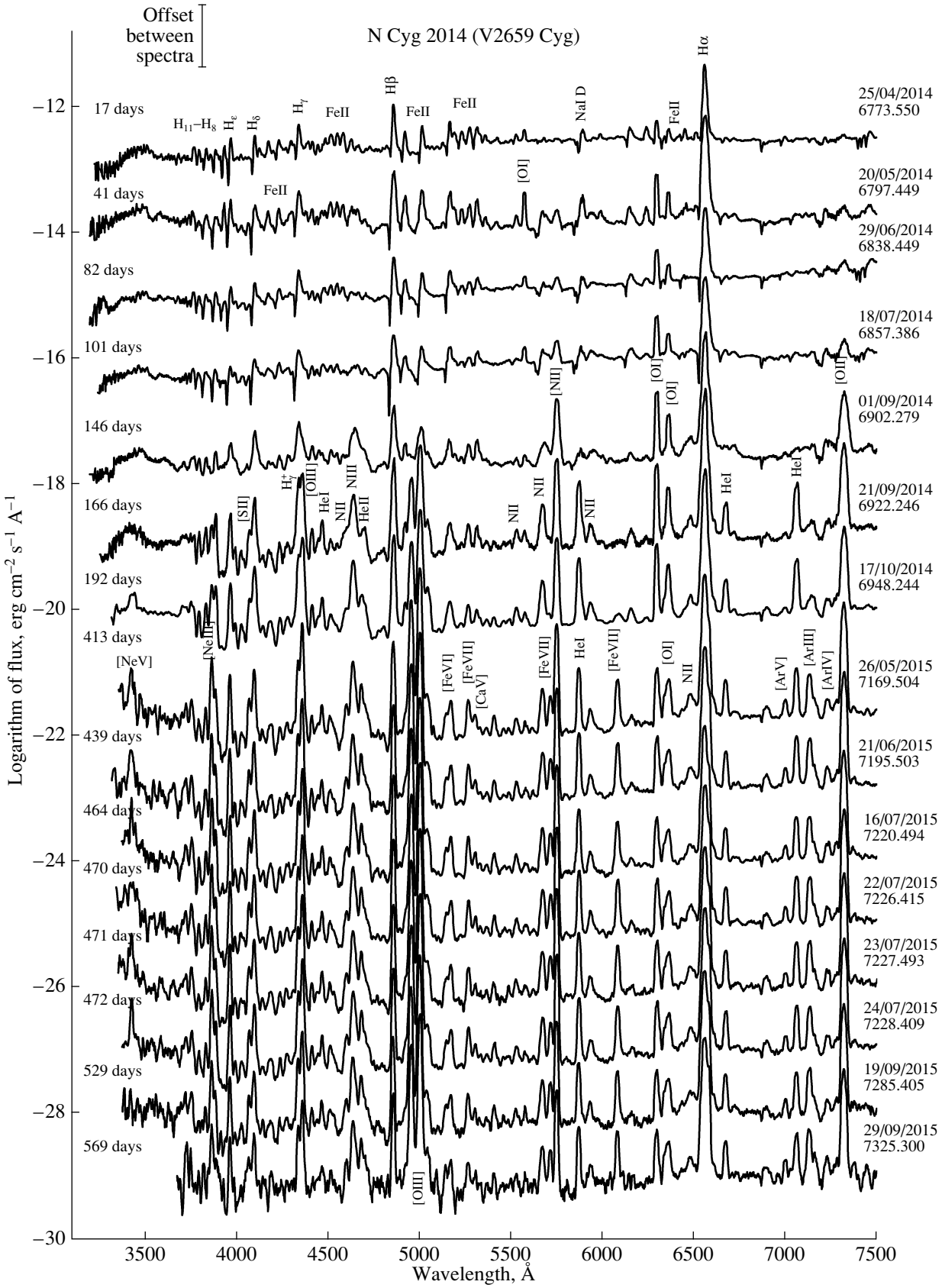

Fig. 2. Low-resolution spectra obtained during the rapid brightness decline 17–569 day after the eruption. The fluxes were not corrected for interstellar absorption and are presented on a logarithmic scale, with successive spectra offset from each other by a constant value. The date and Julian Date (JD 2450000) of the observations are indicated to the right of each spectrum, and the number of days since brightness maximum to the left.

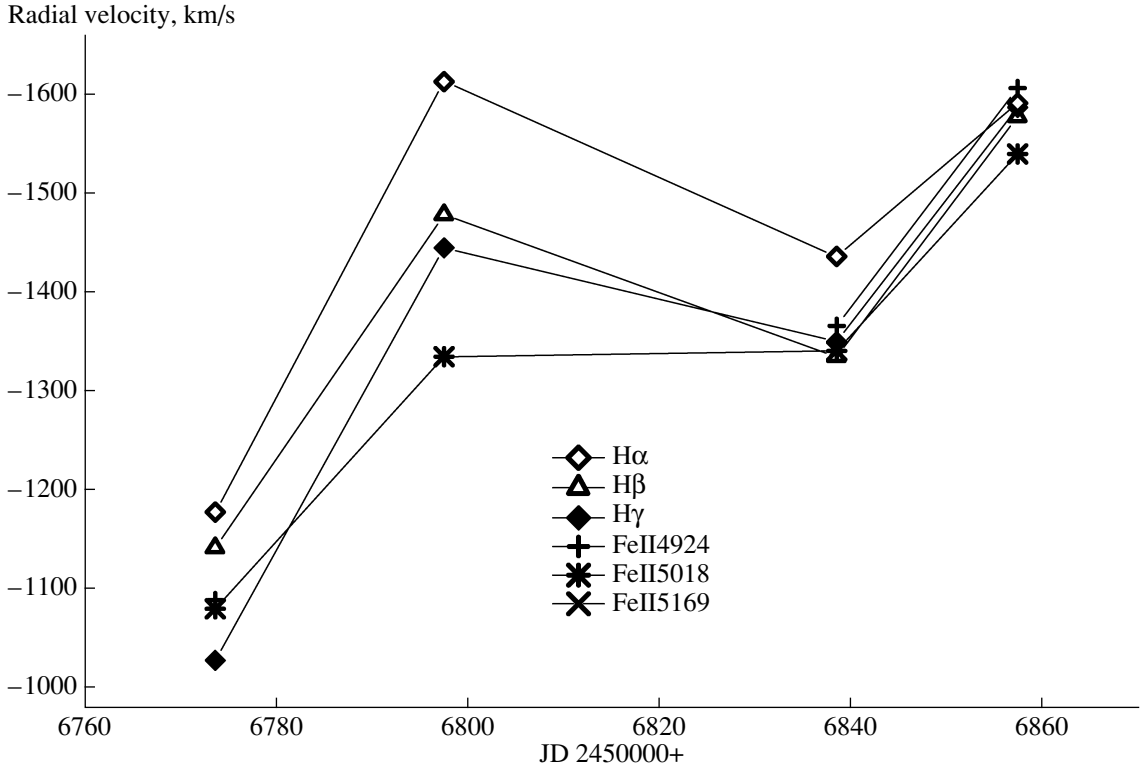

Fig. 3. Radial velocities of the absorption minima of the H_α, H_β, H_γ, and FeII 4924, 5018, and 5169 Å line profiles.

The first four spectra were obtained when chaotic variability was observed in the light curve. The first spectrum was obtained during a period of brightening on the 17th day after the brightness maximum, and the second when the brightness had declined by 1.1^m on the 41st day after the brightness maximum. The third spectrum again corresponds to a brightening (on the 82nd day after maximum), while the fourth was taken after the brightness had again declined by almost 1^m (101 days after the maximum). Our subsequent spectra, starting from the 146th day after maximum, were obtained as the brightness gradually declined, and nova entered the nebular phase.

In addition to HI lines, the first four spectra in Fig. 2 (17–101 days after the eruption) contain lines of ionized iron FeII. The line profiles have well defined P Cygni-type shapes. Lines of the Na I D1+D2 sodium doublet are also present. Fairly strong [OI] 6300, 6363 Å lines appeared on the 41st day (the second spectrum in Fig. 2), as well as a fairly strong [OI] 5577 Å line. This line later significantly weakened and then disappeared on days 82 and 101. The presence of this line simultaneously with the [OI] 6300 and 6364 Å lines shows the presence of structures with densities differing by almost two orders of magnitude in the shell containing neutral oxygen, since the critical density for the [OI] 6300 and 6364 Å lines is of order 10^6 cm^{-3}, while the critical density for the [OI] 5577 Å line is of order 10^8 cm^{-3}.

We used the ratio of the fluxes in [OI] 6300 and 6364 Å lines, which was close to 2.5, to derive the optical depth, which was close to 0.6. We also estimated the optical depth in the [OI] 6364 Å line between days 82 and 166, when the line was only insignificantly blended, to be in range from 0.6 to 0.35.

We determined the radial velocities of the absorption components of the HI lines and analyzed their time variations, shown in Fig. 3. The absorption minima of the H_α, H_β, and H_γ lines in the first spectrum, obtained on the 17th day after the brightness maximum during a period of brightening, are shifted toward the blue by 1180, 1140, and 1030 km/s, respectively, while the absorption minima of the FeII 5018, 4923, and 5169 Å lines are shifted by about 1100 km/s. In the following spectrum, obtained 41 days after the brightness maximum, when the brightness had declined, the radial velocity of the H_α absorption component had increased to 1610 km/s, the radial velocities of H_β and H_γ to 1480 km/s, and the radial velocities of the iron lines to 1340

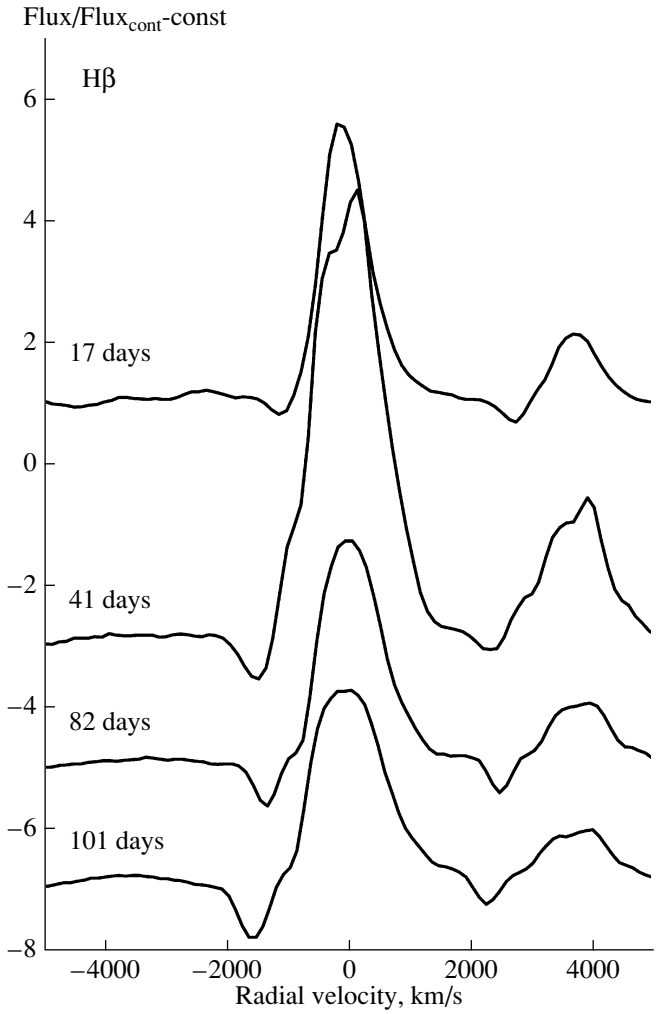

Fig. 4. Changes in the shape of the H_β profiles during the period of chaotic brightness fluctuations (days 17–101 after eruption). The spectra are normalized to the continuum and offset from each other by a constant value.

and 1500 km/s. During the next brightening, in the spectrum obtained 82 days after the brightness maximum, the radial velocities of the absorption components decreased slightly, to 1440 km/s for H_α and almost 1350 km/s for the other lines. In the spectrum obtained 101 days after the maximum, during the brightness decline, the absorption radial velocities increased again, to 1500–1600 km/s.

Figures 4 and 5 show the H_β and FeII 5018 Å profiles. During the brightness decline (41 and 101 days after the maximum), the increase in the velocity of the absorption components was accompanied by changes in the shapes of the line profiles. Despite the low spectral resolution, it is clear that the line profiles became multi-component. The most appreciable changes were observed on the 41st day, when the brightness had declined by almost 1^m compared to the maximum. On this date, the intensity of the emission component was the highest, and the shape of the line profile changed appreciably. The H_β and FeII 5018 Å lines became more complex, with multiple components. Furthermore, the FeII absorption components almost disappeared on this date. The FeII line profile also became more complex 101 days after the maximum, during the next fading (Fig. 5). The multi-component structure of the H_β profile on this date is not obvious, but it is clear that the profile became significantly broader.

The fifth spectrum, obtained on the 146th day, shows that the nova was in the early phase of the nebular stage. The NII + NIII 4640 Å + HeII 4686 Å blend and forbidden lines of ionized nitrogen [NII] 5755 Å and oxygen [OII] 7320, 7331 Å appeared in the spectrum.

The next two spectra were obtained during the developed nebular stage, when the strongest line,

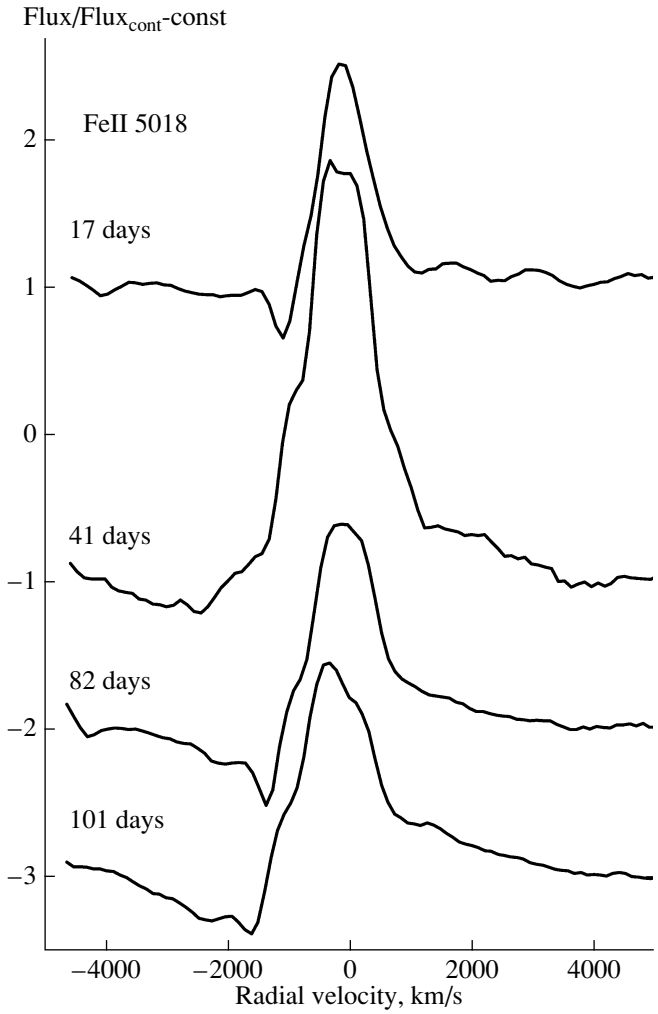

Fig. 5. Same as Fig. 4 for the FeII 5018 Å line.

apart from H_α, was the [OIII] 5007 Å forbidden line. The HeI 5876, 6678, 7065 Å recombination lines and NII 5535, 5680, 5938 Å lines appeared in the spectrum, which also contained the [OIII] 4363 Å line, which forms a blend with H_γ, and the [OIII] 4959 Å and [NeIII] 3869, 3968 Å lines, with the latter forming a blend with H_ϵ. There was also a strong [ArIII] 7136 Å line. Lines with high ionization potentials had appeared in the specrum 413 days after the brightness maximum: [NeV] 3426, [FeVI] 5176, [FeVII] 5721, 6086, [CaV] 5309, [ArIV] 7236, [ArV] 7006 Å, and the HeII 4686 Å line became stronger. The line profiles evolved only slightly in the nebular stage, and displayed complex shapes only on days 166 and 192; they later acquired a rounded shape. Figures 6 and 7 illustrate this behavior of the line profiles using the H_β and [OIII] 5007 Å profiles as examples, and Fig. 8 presents the [FeVII] 6086 Å profiles, which also have rounded shapes. Figure 9 presents the variations of the line full-width at half maximum (FWHM) intensity, which show that the mean velocity of the shell expansion, given by the line FWHM, varied approximately between 660 km/s (146th day) and 480 km/s (569th day).

5. CHEMICAL COMPOSITION AND MASS OF THE SHELL

5.1. Chemical Composition of the Shell

In order to estimate elemental abundances, we calculated the line fluxes on dates when the nova was in the developed nebular stage (days 413–569). These fluxes are presented in Table 2. Average fluxes are presented for 470–472 days, 529 days, and 569 days after the maximum brightness (July 22–24, September 19, and October 29, 2015). The flux errors are 20 to 50%. Interstellar reddening

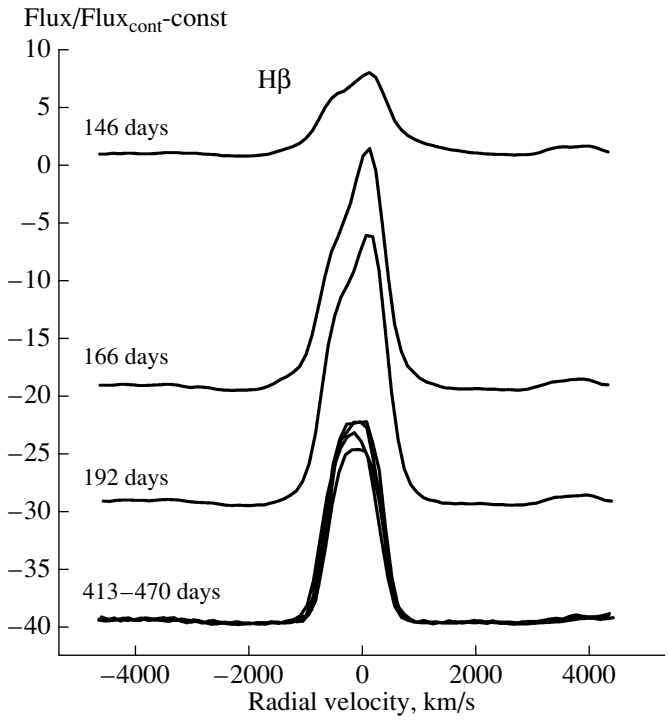

Fig. 6. Variations of the H_β line shape in the nebular stage (days 146–470 after the beginning of the eruption). The presentation of the spectra is the same as in Fig. 4.

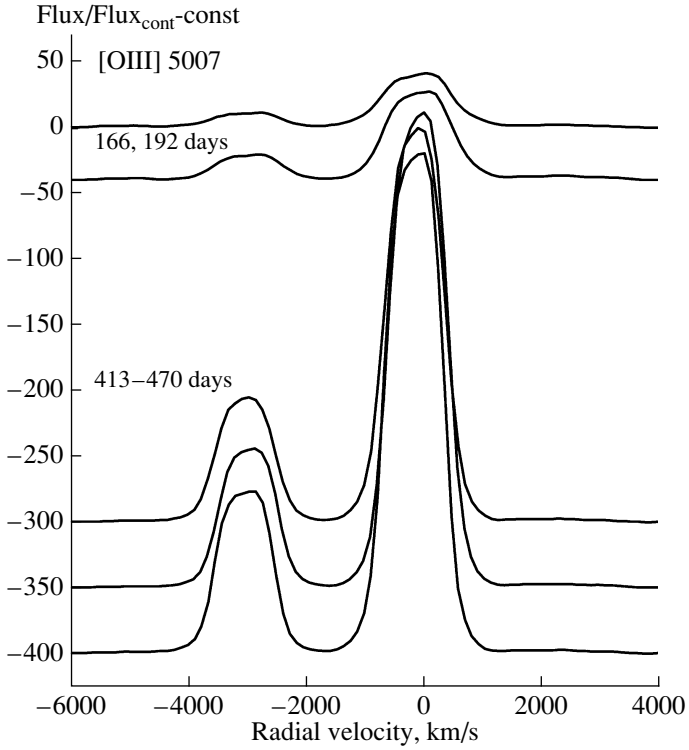

Fig. 7. Variations of the [OIII] 5007 Å line profile shape in the nebular stage (days 166–470 after the beginning of the eruption). The presentation of both spectra is the same as in Fig. 4.

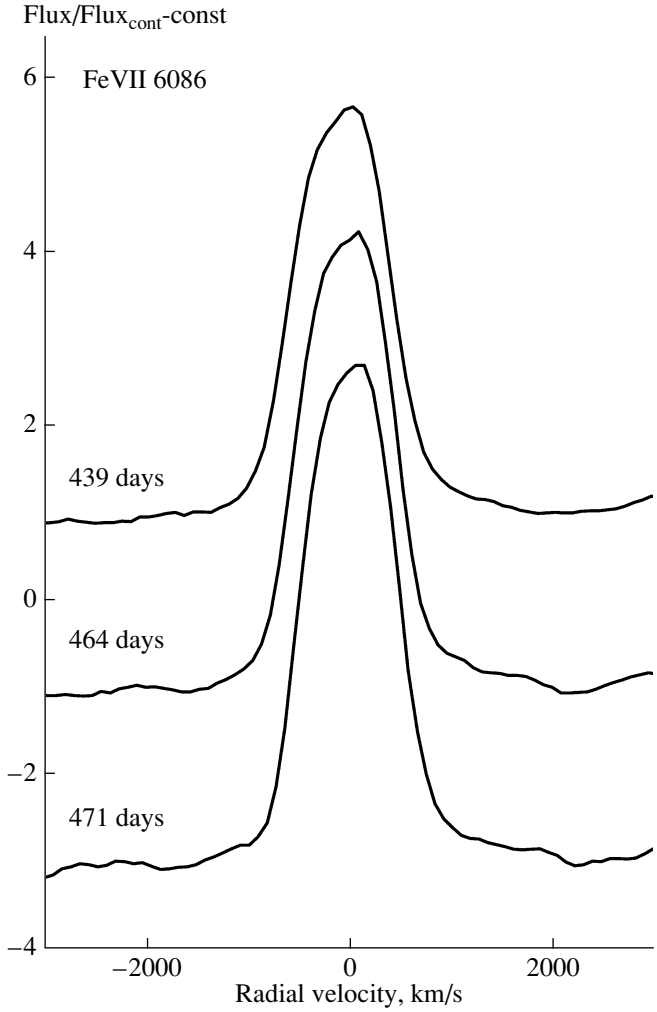

Fig. 8. [FeVII] 6086 Å line profiles. The presentation of the spectra is the same as in Fig. 4.

was taken into account in the flux calculations. We calculated the color excess $E(B-V)$ by comparing the observed and theoretical ratios of the H_α and H_β fluxes, taking the theoretical ratio to be 2.81. The calculated color excess was 1.64. Color excess have also been calculated in other studies. Tomov et al. [6] found a larger value, $E(B-V) = 2.10 \pm 0.23$. The values of $E(B-V)$ found by Chochol et al. [5] are 0.92 and 0.85, while Raj et al. [7] found an even lower value, 0.63. As the methods used to obtain the color excesses were different, we adopted the average value $E(B-V) = 1.23$.

Determining elemental abundances requires estimation of the electron temperature and matter density in the nova shell. The temperature of the nova shell was obtained by comparing the theoretical and observed ratios of the fluxes in the [OIII] 5007+4959 and [OIII] 4363 Å, [FeVI] 5176 and [FeVI] 5146 Å, [NII] 5755 and [OII] 7325 Å lines. We used the NEBULAR.IONIC code [8] to find the density dependence of the temperature for densities from 10^5 to 10^7 cm^{-3} and the average observed flux ratio of 11. A second density dependence for the temperature was derived using the ratio of the fluxes in the [FeVI] 5176 and [FeVI] 5146 Å lines. The observed line-flux ratios lie between 1.9 and 2.05, with a mean value of 1.76. The theoretical flux ratios for the [FeVI] 5176 and [FeVI] 5146 Å lines were taken from [9]. We also used the relations derived for the ratios of the fluxes in the [NII] 5755 Å line and the [OII] 7325 Å blend in [10] to estimate the density and temperature.

Comparing the density dependence of the temperature for the ratios of the [OIII] 5007+4959 and [OIII] 4363 Å, [FeVI] 5176 and [FeVI] 5146 Å, and [NII] 5755 and [OII] 7325 Å fluxes yielded temperatures between 11 000 and 7000 K and electron densities between 10^5 and 10^7 cm^{-3}. When calculating elemental abundances, we adopted the temperature

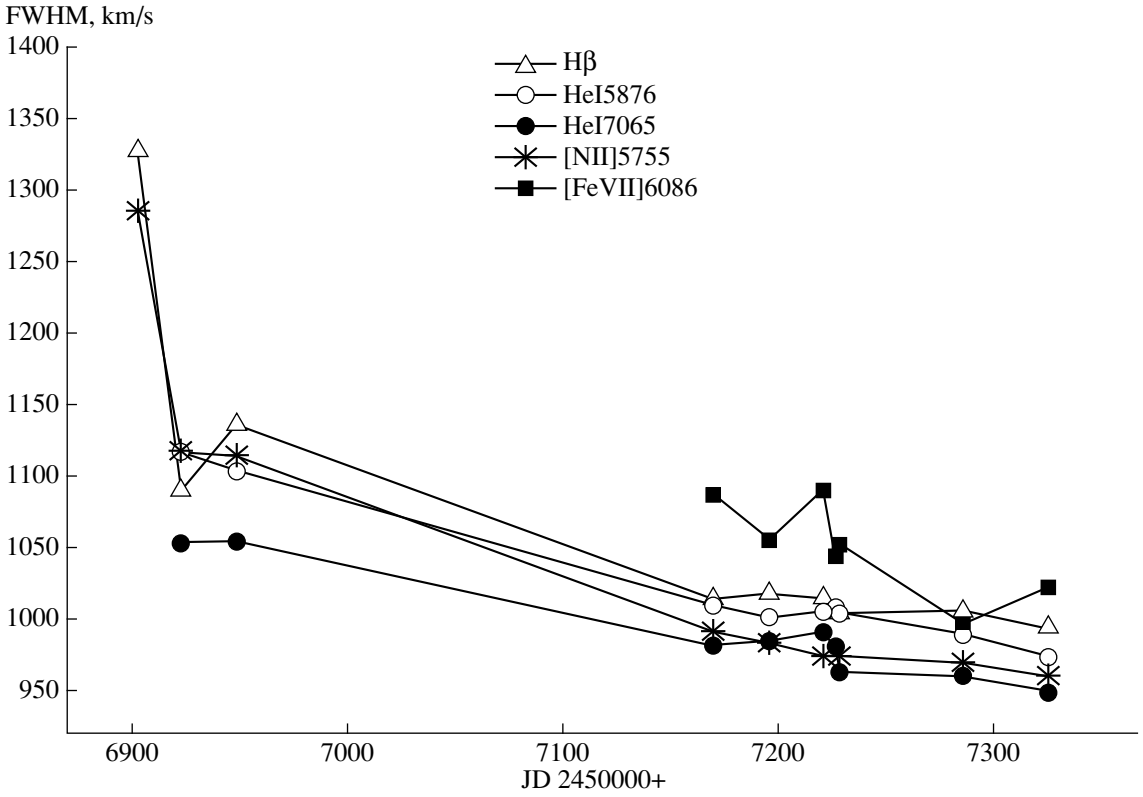

Fig. 9. FWHM of the spectral lines.

9000 K and the density 5×10^6 cm^{-3}, as an intermediate value between 10^5 and 10^6 cm^{-3}. We did not consider the higher density $\approx 10^7$ cm^{-3}, since, at such densities, the forbidden nitrogen lines [NII] 6584, 6548 Å, whose critical density for a temperature of about 10 000 K is of order 10^5 cm^{-3}, should be absent from the spectrum. However, though they are not very strong, these lines are confidently detected, forming a blend with the H_α line. A temperature of 9000 K was adopted as an average temperature in the above range. In addition to the selected density and temperature ($N_e = 5 \times 10^6$ cm^{-3}, $T_e = 9000$ K), we calculated elemental abundances for two more sets of electron density and temperature (5×10^6 cm^{-3}, 11 000 K) and (10^5 cm^{-3}, 9000 K), in order to estimate the uncertainties in the abundances due to our chosen average density and electron temperature. The difference between the abundance estimates obtained for these various physical conditions was taken to be the uncertainty in these estimates. We also took there to be an additional error due to the uncertainties in the measured line fluxes, which were, as a rule, between 20 and 50%. We took the estimated density and temperature to be the average values 413–569 days after the brightness maximum, assuming that the physical conditions in the shell remained constant during this time.

Below, we present relationships by means of which the elemental abundances relative to hydrogen were estimated. The abundances of ions with permitted lines were determined from the relationship

$$\frac{N(X^{i+})}{N(H^+)} = \frac{\lambda(X^{i+})}{\lambda(H_\beta)} \frac{\alpha^{\text{eff}}(H_\beta)}{\alpha^{\text{eff}}(\lambda)} \frac{I(\lambda)}{I(H_\beta)}, \qquad (1)$$

where $\alpha^{\text{eff}}(H_\beta)$ and $\alpha^{\text{eff}}(\lambda)$ are recombination coefficients, and $I(\lambda)$ and $I(H_\beta)$ are the observed intensities of a line with wavelength $\lambda(X^{i+})$ and the H_β line.

We used the HeI 5876 and HeII 4686 Å lines to estimate the helium abundance. The relationship used to determine the helium-ion abundance was taken from [11]. When calculating the helium-ion abundance using the HeI 5876 Å line, we included the effect of collisional excitation of the metastable $2S^2\ ^3S$ HeI level [12].

The following relationships were used to estimate the helium-ion abundance using the HeI 5876 and HeII 4686 Å lines:

$$\log \frac{N(He^+)}{N(H^+)} = -0.133 + 0.235 \times \log(t_e) + \log \frac{I(5876)}{I(H_\beta)}, \qquad (2)$$

Table 2. Emission-line fluxes for V2659 Cyg in 2015 413–569 days after the beginning of the eruption (in 10^{-13} erg cm^{-2} s^{-1}).

Line, Å	27.05	22.06	16.07	22–24.07	19.09, 29.10
[NeIII] 3869	485	290	263	240	178
H_8	129	76	70	64	49
H_ϵ + [NeIII] 3968.7	232	156	120	118	91
H_δ	269	197	156	139	106
H_γ	270	187	149	148	115
[OIII] 4363.0	1122	685	525	496	305
HeI 4471.5	31	21	18	18	15
NIII 4640	312	218	181	173	154
HeII 4685.7	95	69	56	55	55
H_β	372	369	277	246	207
[OIII] 4958.9	1706	1640	1503	1226	1257
[OIII] 5006.8	5276	4893	4420	3686	3733
[FeVI] 5146.8	16	15	12	10	9
[FeVI] 5177.0	31	30	20	19	17
[FeVI] 5279	27	26	17	15	11
[CaV] 5308.9	11	11	6	5	4
NII 5667,80	34	32	20	21	18
[FeVII] 5720.9	20	19	13	13	12
[NII] 5754.8	330	308	185	189	137
HeI 5875.6	61	57	33	35	31
[FeVII] 6087 + [CaV] 6086.9	36	35	18	20	19
[OI] 6300.2	49	39	19	21	20
[OI] 6364 + [FeX] 6374.5	36	24	12	14	14
H_α + NII 6482.1, 6583.6	1815	1306	731	896	945
HeI 6678	24	16	10	11	11
[ArV] 7005.7	6	5	2	3	3
HeI 7065	33	28	13	14	13
[ArIII] 7135.8	27	26	14	15	16
[ArIV] 7236.0	6	4	3	3	4
[OII] 7319.4, 30.7	406	320	176	195	162

$$\log\frac{N(\mathrm{He}^{++})}{N(\mathrm{H}^{+})} = -1.077 + 0.135\times\log(t_e) + \frac{0.135}{t_e} + \log\frac{I(4686)}{I(\mathrm{H}_\beta)}, \quad (3)$$

where $t_e = T_e/10^4$ K, and $I(5876)$ and $I(4686)$ are the observed intensities of the HeI 5876 and HeII 4686 Å lines. The total helium abundance was found by summing the abundances of the He^+ and He^{++} ions. The ionization state He^0 was not taken into account, since it was assumed that all the helium in the nova shell was ionized.

When forbidden lines were used, the abundances

of ions were derived using the relationship

$$\frac{N(\mathrm{X}^i)}{N(\mathrm{H}^+)} = \frac{I(\lambda)}{I(\mathrm{H}_\beta)}\frac{j(\mathrm{H}_\beta)}{j(\lambda)}, \quad (4)$$

where $I(\mathrm{H}_\beta)$ and $I(\lambda)$ are the line intensities and $j(\mathrm{H}_\beta)$ and $j(\lambda)$ the volume emission coefficients for the H_β line and a forbidden line with wavelength λ. The NEBULAR.IONIC code [8] calculates the emissivity of the forbidden line and the H_β line for a given temperature and density, then calculates the abundances of the ions relative to hydrogen, based on the observed intensities of the forbidden lines, normalized to the H_β intensity. We used this code to determine the nitrogen, oxygen, neon, argon abundances.

We estimated the abundances of iron ions using the [FeIV] 5176 and [FeVII] 6087 Å lines, for which relationships for the emissivity were taken from [9, 13]. We used the permitted NII 5680 and NIII 4640 Å lines and the forbidden [NII] 5755 Å line to determine the abundances of nitrogen ions. We calculated the nitrogen abundance using the permitted lines together with the following relationship:

$$\frac{N(\mathrm{X}^{i+})}{N(\mathrm{H}^+)} = X_i(T_e)\frac{I(\lambda)}{I(\mathrm{H}_\beta)}, \quad (5)$$

where $X_i(T_e) = \chi_0 t^\eta$ and $t = T_e/10^4$ K. The coefficients χ_0 and η were taken from [14]. For NII 5680 Å, $\chi_0 = 0.205$ and $\eta = -0.41$, while for NIII 4640 Å, $\chi_0 = 0.014$ and $\eta = -0.71$.

We determined the elemental abundances by either summing the abundances of ions in the different ionization states, or using ionization correction coefficients (ICFs). An ICF is applied when there is no complete set of ions of an element in successive ionization states that can be used to determine the abundance. In this case, ICFs can be used to take into account the contribution of missing ions to the overall abundance.

The oxygen, nitrogen, and argon abundances were determined using the two methods, while the neon and iron abundances were obtained using ICFs only. The ICF relations for oxygen and nitrogen were taken from [11], those for argon and neon from [15], and those for iron from [16].

The relationships used to obtain the total elemental abundances are given below. For oxygen:

$$\frac{\mathrm{O}}{\mathrm{H}} = \frac{\mathrm{O}^0(6300) + \mathrm{O}^+(7325) + \mathrm{O}^{++}(5007)}{\mathrm{H}^+(\mathrm{H}_\beta)}, \quad (6)$$

$$\frac{\mathrm{O}}{\mathrm{H}} = \frac{\mathrm{O}^+(7325) + \mathrm{O}^{++}(5007)}{\mathrm{H}^+(\mathrm{H}_\beta)}\mathrm{ICF}, \quad (7)$$

where

$$\mathrm{ICF} = \frac{\mathrm{He}^+(5876) + \mathrm{He}^{++}(4686)}{\mathrm{He}^+(5876)}. \quad (8)$$

The oxygen abundances determined using the different methods differ only insignificantly.

For nitrogen:

$$\frac{\mathrm{N}}{\mathrm{H}} = \frac{(\mathrm{N}^+(5755) + \mathrm{N}^{2+}(5680))/2 + \mathrm{N}^{3++}(4640)}{\mathrm{H}^+(\mathrm{H}_\beta)}, \quad (9)$$

$$\frac{\mathrm{N}}{\mathrm{H}} = \frac{\mathrm{N}^+(5755)}{\mathrm{H}^+(\mathrm{H}_\beta)}\mathrm{ICF}, \quad (10)$$

where

$$\mathrm{ICF} = \frac{\mathrm{O}^+(7325) + \mathrm{O}^{++}(5007)}{\mathrm{O}^+(7325)}. \quad (11)$$

The nitrogen abundance derived using the NII 5680 and NIII 4640 Å permitted lines differs from the abundance derived using the [NII] 5755 Å forbidden line by more than an order of magnitude. This pattern was also observed by Arkhipova et al. [17] and in our earlier papers [18–20]. It was suggested in those studies that this difference could be due to the fact that these lines form in different regions of the shell. Table 3 presents the mean nitrogen abundance obtained using the two methods. For argon:

$$\frac{\mathrm{Ar}}{\mathrm{H}} = \frac{\mathrm{Ar}^{++}(7136) + \mathrm{Ar}^{2+}(7237) + \mathrm{Ar}^{3+}(7006)}{\mathrm{H}^+(\mathrm{H}_\beta)}, \quad (12)$$

$$\frac{\mathrm{Ar}}{\mathrm{H}} = \frac{\mathrm{Ar}^{++}(7136)}{\mathrm{H}^+(\mathrm{H}_\beta)}\mathrm{ICF}, \quad (13)$$

where

$$\mathrm{ICF} = \frac{\mathrm{N}}{\mathrm{N}^{2+}(5680)}, \quad (14)$$

and

$$\frac{\mathrm{Ar}}{\mathrm{H}} = \frac{\mathrm{Ar}^{3+}(7006)}{\mathrm{H}^+(\mathrm{H}_\beta)}\mathrm{ICF}, \quad (15)$$

where

$$\mathrm{ICF} = \frac{\mathrm{He}}{\mathrm{He}^{++}(4686)}. \quad (16)$$

The argon abundance derived from the [ArIII] 7136 and ArV 7006 Å lines using the ICF is lower than the mean abundance derived from the [ArIII] 7136, ArV 7006, and [ArIV] 7237 Å lines. This may come about because the argon abundance obtained

Table 3. Ion abundances in the shell of V2659 Cyg (logarithmic scale)

Ion	Abundance
He^{+}/H	-0.96 ± 0.13
He^{++}/H	-1.59 ± 0.18
N^{+}/H	-2.98 ± 0.25
N^{+}/H	-1.74 ± 0.20
N^{++}/H	-1.99 ± 0.20
O^{0}/H	-3.96 ± 0.30
O^{+}/H	-1.89 ± 0.35
O^{++}/H	-2.16 ± 0.35
Ne^{++}/H	-3.68 ± 0.24
Ar^{++}/H	-5.78 ± 0.27
Ar^{2+}/H	-5.01 ± 0.38
Ar^{3+}/H	-6.42 ± 0.30
Ca^{3+}/H	-5.81 ± 0.30
Fe^{5+}/H	-4.94 ± 0.57
Fe^{6+}/H	-4.92 ± 0.52

from the [ArIV] 7237 Å line is overestimated because the CII 7236 Å may contributes to the flux, as in the nova V339 Del. However, in the case of V339 Del, this line was very strong before the nebular stage. Therefore, when deriving our final argon abundance for V2659 Cyg, we did not include the contribution of the [ArIV] 7237 Å line. In the case of V2659 Cyg, we are not sure that the CII 7236 Å line makes a significant contribution to the flux, and we thus adopted the average of the abundances obtained using the different methods for our final argon abundance.

For neon:

$$\frac{\mathrm{Ne}}{\mathrm{H}} = \frac{\mathrm{Ne}^{++}(3869)}{\mathrm{H}^{+}(\mathrm{H}_{\beta})}\mathrm{ICF}, \qquad (17)$$

where

$$\mathrm{ICF} = \frac{\mathrm{O}^{+}(7325) + \mathrm{O}^{++}(5007)}{\mathrm{O}^{++}(5007)}. \qquad (18)$$

For iron:

$$\frac{\mathrm{Fe}}{\mathrm{H}} = \frac{\mathrm{Fe}^{5+}(5176) + \mathrm{Fe}^{6+}(6087)}{\mathrm{H}^{+}(\mathrm{H}_{\beta})}\mathrm{ICF}, \qquad (19)$$

where

$$\mathrm{ICF} = \frac{\mathrm{He}^{+}(5876) + \mathrm{He}^{++}(4686)}{\mathrm{He}^{++}(4686)}. \qquad (20)$$

Table 4. Abundance of some elements in the shell of V2659 Cyg relative to the solar values (in dex)

Element	Abundance
[He/H]	0.11 ± 0.18
[N/H]	$2.54/2.45/1.15 \pm 0.25$
[O/H]	$1.61/1.70 \pm 0.35$
[Ne/H]	0.78 ± 0.25
[Ar/H]	$0.67 \pm 0.38/-0.1 \pm 0.30/-0.15 \pm 0.27$
[Fe/H]	0.63 ± 0.5

Our derived iron abundance exceeds the solar value. This probably suggests that the temperature of the zone where the [FeVII] 6087 Å forms is higher. Indeed, for a temperature of 17 000 K, we obtained an iron abundance that almost coincides with the solar value. Table 3 also presents the iron abundances for temperatures of 9000 K and 17 000 K.

We also derived the abundance of the calcium ion Ca^{3+} 5309 Å, using the following ratio from [11]:

$$\frac{N(\mathrm{Ca}^{3+})}{N(\mathrm{H}^{+})} = 2.6 \times 10^{-6}\, E^{0}_{4,2}\sqrt{t} \times 10^{1.14/t}\frac{I(5309)}{I(\mathrm{H}_{\beta})}, \qquad (21)$$

where

$$E^{0}_{4,2} = 1.24t^{-0.87}. \qquad (22)$$

Table 3 presents (on a logarithmic scale) our estimated abundances of helium, nitrogen, oxygen, neon, argon, iron, and calcium averaged over all observing epochs. Our estimates of the total abundances of helium, nitrogen, oxygen neon, argon, and iron relative to the solar values are presented in Table 4. The values obtained using the different methods are separated by slashes.

To compare the abundances of some elements in V2659 Cyg with those for other FeII novae, which are supposed to harbor a carbon–oxygen (CO) white-dwarf accretor, we present all abundances available in the literature relative to the solar values in Fig. 10 [16–21]. The elemental abundances for V2659 Cyg are marked by filled circles in Fig. 10. The neon and oxygen abundances for V2659 Cyg stand out, as they are nearly the highest among all the presented values. A similar oxygen abundance is observed only for V1668 Cyg, and a higher neon abundance only for V977 Sco. However, the nitrogen abundance of V2659 Cyg does not differ from those for the other novae, and its value is close to the lowest nitrogen abundances in the CO novae shown in Fig. 10. Only

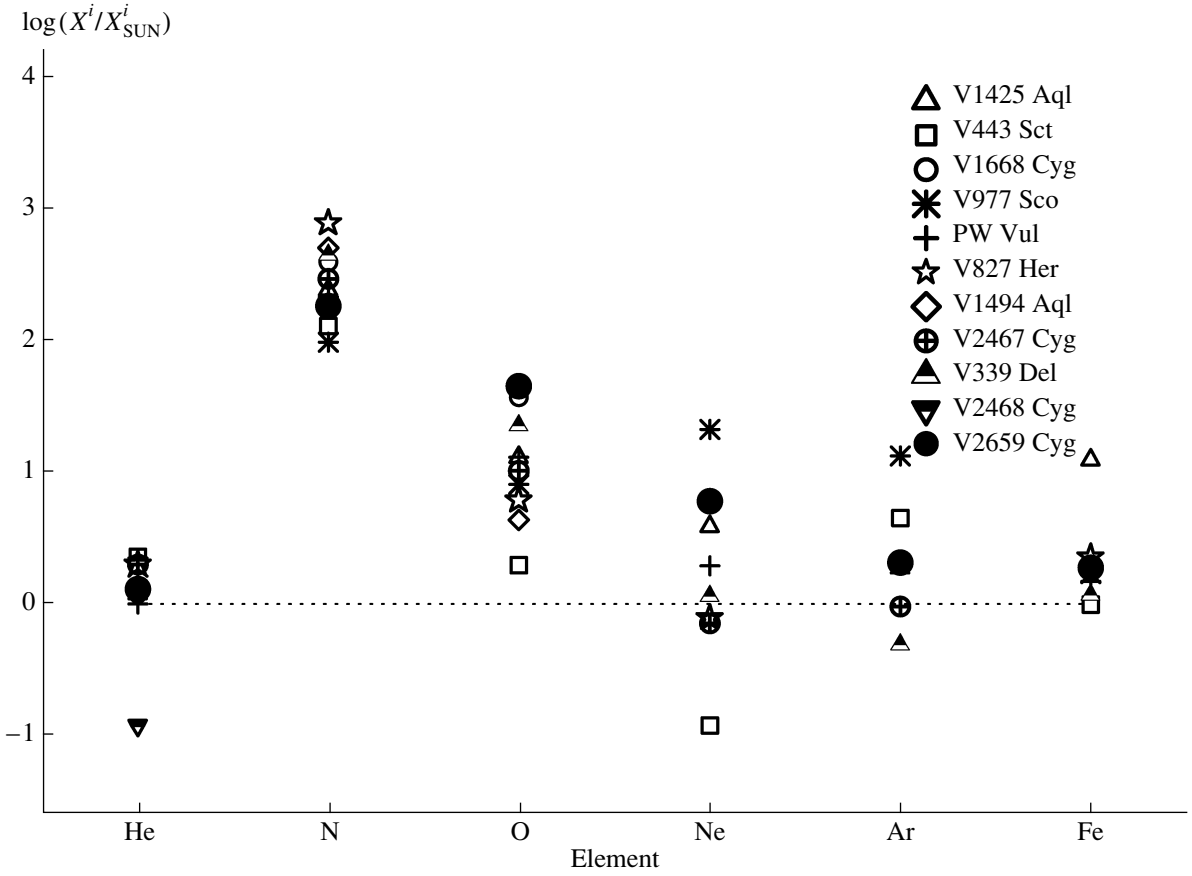

Fig. 10. Elemental abundances in 11 novae with CO white dwarfs. The values for V2659 Cyg are marked by filled circles. The dashed line shows the solar abundances.

V977 Sco and V443 Sct have lower nitrogen abundances.

Note that we have obtained only rough estimates of the abundances of some elements in the nova shell, because we did not take into account the heterogeneity of the shell temperature and density.

5.2. Mass of the Shell

We determined the mass of the emitting hydrogen envelope as $M = n_e m_{\rm H} V$. The volume of the shell was found by comparing the observed and theoretical H_β luminosities of the nova: $4\pi D^2 F_{H_\beta} = 4\pi\epsilon_{H_\beta} V$. This yielded $M = 7.99 F_{H_\beta} D^2 t_e^{0.85} n_e^{-1}\ M_\odot$, where $4\pi\epsilon_{H_\beta} = 1.24\times10^{-25} t_e^{-0.85} n_e n_{H+}$ is the emissivity in the H_β line, $m_{\rm H} = 1.64\times10^{-24}$ g the mass of a hydrogen atom, $F_{H_\beta} = 2.94$ the H_β flux averaged over our observing epochs in units of 10^{-11} erg cm^{-2} s^{-1}, D the distance to the nova, t_e the electron temperature of the shell normalized to 10^4 and equal to 0.9, n_e the electron density, which is equal to the average electron density calculated using our data, 5×10^6 cm^{-3}, and $M_\odot$ the solar mass. The distance $D = 5.5$ kpc was taken from [5]. This yielded a mass for the hydrogen shell of $1.3\times10^{-4}\ M_\odot$. We found the total mass of the shell by taking into account the fact that, according to our estimates, the mass fraction of hydrogen in the nova shell is $X = 0.475$; this yields a total mass of the shell of $2.7\times10^{-4}\ M_\odot$.

Using the ratio of the [OI] 6300 and 6364 Å fluxes, which is close to 2.5, we found the optical depth of the shell to be ∼0.6 and the temperature of the region of the shell where neutral oxygen is formed to be ∼5800 K. Knowing the temperature and optical depth, we determined the mass of neutral hydrogen in the shell to be $9\times10^{-5}\ M_\odot$. The expressions used to calculate the optical depth, temperature, and mass of neutral oxygen in the nova shell were taken from [22]. When estimating the mass of oxygen, the volume occupied by the oxygen was calculated by comparing the observed and theoretical luminosities. The mass of neutral oxygen in this case is the total mass of oxygen, because we estimated it in a phase when all the oxygen was in the neutral state (there were no lines of ionized oxygen in the spectrum). The expressions used to calculate the optical depth,

Table 5. Main parameters of V2659 Cyg

Parameter	Value
JD_{max}	$\approx$2456757.943
V_{max}	9.3–9.4^m
$M_{V\,max}$	-6.7 ± 0.04^m [5]
Velocity class	moderately fast $t_2 \approx 60$–65^d [5] $t_3 \approx 150^d$
Distance, kpc	5.5 ± 0.3 [5]
Average color $E(B-V)$ excess	1.2
Mass of the white dwarf, $M_\odot$	0.65 ± 0.02 [5]
Spectral class	FeII
Type of the white dwarf	CO
Max. velocity of the shell expansion, km/s	$\approx 1600 \pm 50$
Average velocity of the shell expansion, km/s	$\approx 600 \pm 50$
Oxygen mass, $M_\odot$	$\approx 1 \times 10^{-4}$
Shell mass, $M_\odot$	$\approx 3 \times 10^{-4}$
Elemental abundances relative to the solar values (dex)	
[He/H]	0.11 ± 0.18
[N/H]	2.26 ± 0.25
[O/H]	1.66 ± 0.35
[Ne/H]	0.78 ± 0.25
[Ar/H]	0.32 ± 0.38
[Fe/H]	0.63 ± 0.50

temperature, and mass of oxygen are:

$$\frac{F(\lambda 6300)}{F(\lambda\,6364)} = \frac{(1-e^{-\tau})}{(1-e^{-\tau/3})}, \quad (23)$$

$$T_e(\mathrm{O}^0) \quad (24)$$
$$= \frac{11200}{\log\left[43\tau/(1-e^{-\tau}) \times F(\lambda\,6300)/F(\lambda\,5577)\right]},$$

$$M(\mathrm{O}^0) \quad (25)$$
$$= 152 D^2 e^{22850/T_e(\mathrm{O}^0)} \frac{\tau}{(1-e^{-\tau})} F(\lambda 6300)\ M_\odot.$$

Here, $T_e(\mathrm{O}^0)$ is the electron temperature in the zone of neutral oxygen, τ the optical depth, D the distance in kpc, $M(\mathrm{O}^0)$ the mass of neutral oxygen in solar units, and $F(\lambda\,6300)$, $F(\lambda\,6364)$, and $F(\lambda\,5577)$ the fluxes in the [OI] 6300, 6364, and 5577 Å lines.

6. CONCLUSION

Table 5 presents the basic photometric and spectroscopic characteristics of the nova, some of which were taken from Chochol et al. [5]. The nova is moderately fast and has spectroscopic class FeII. The binary harbors a relatively low mass CO white dwarf ($0.65\ M_\odot$). The mean rate of expansion of the shell in the nebular stage is low: on average, about 500 km/s. Table 5 shows that the nova has higher than solar abundances of nitrogen, oxygen, neon, argon, and iron: $[\mathrm{N/H}] = 2.26 \pm 0.25$, $[\mathrm{O/H}] = 1.66 \pm 0.35$, $[\mathrm{Ne/H}] = 0.78 \pm 0.25$, $[\mathrm{Ar/H}] = 0.32 \pm 0.38$, and $[\mathrm{Fe/H}] = 0.63 \pm 0.5$ dex. We suggest that the enhanced iron abundance indicates that we must assume a higher temperature when estimating this abundance, consistent with the [FeVII] line forming in a zone with a higher temperature. If a temperature of 17 000 K is assumed, the estimated iron abundance becomes close to the solar value. The nova V1668 Cyg stands out among similar novae due to its relatively high oxygen and neon and low nitrogen abundances. The mass of the emitting shell we derived is high, about $3 \times 10^{-4}\ M_\odot$. We also estimated the electron temperature and mass of neutral oxygen in the nova shell to be $T_e(\mathrm{O}^0) = 5800$ K and $\approx 10^{-4}\ M_\odot$.

An interesting feature of nova is chaotic brightness variations prior to the nebular stage. Our spectroscopic observations were obtained during periods of increasing brightness 17 and 82 days after the maximum of the eruption and during a decrease in the brightness by $\approx 1^m$ 41 and 101 days after the maximum. Over this period, the HI and FeII lines had P Cygni profiles, during periods of both increasing and decreasing brightness. However, the depths and radial velocities of the absorption components changed. We did not note any pattern in the variations of the depths of the absorption components. However, their radial velocities increased as the brightness decreases, on average, by $\approx$ 400 km/s on day 41 and $\approx$ 200 km/s on day 101, reaching 1600 km/s in both cases. We also found that the shapes of the HI and FeII emission profiles changed on these dates, becoming more complex (multi-component), and a significant increase in the intensity of these components was also observed on day 41.

ACKNOWLEDGMENTS

We thank all the observers who contributed to the creation of the worldwide AAVSO database for the possibility of using their observations in our study.

REFERENCES

1. K. Nishiyama, F. Kabashima, G. Masi, F. Nocentini, P. Schmeer, W. Vollmann, U. Munari, G. Cetrulo, D. Degano, F. Castellani, A. Arai, K. Ayani, and M. Fujii, Centr. Bur. Electron. Telegrams, No. 3842, 1 (2014).
2. E. V. Kazarovets and N. N. Samus, Var. Stars **35**, No. 3 (2015).
3. V. I. Burnashev, Byull. Abastum. Astrofiz. Observ. **59**, 83 (1985).
4. K. Imamura, H. Akazawa, and H. Maehara, Astron. Telegram, No. 6128 (2014).
5. D. Chochol, N. Ikonnikova, N. Katysheva, S. Shugarov, and I. Volkov, in *Living Together: Planets, Host Stars and Binaries,* Ed. by S. M. Rucinski, G. Torres, and M. Zejda, ASP Conf. Ser. **496**, 237 (2015).
6. T. Tomov, E. Swierczynski, D. Puchalski, D. Dimitrov, D. Chanliev, A. Kurtenkov, T. Bonev, D. Marchev, and D. Kjurkchieva, Astron. Telegram, No. 6060 (2014).
7. A. Raj, U. Munari, B.-C. Lee, S. C. Kim, S.-J. Kim, and C.-K. Sim, Astron. Telegram, No. 6181 (2014).
8. R. A. Shaw and R. J. Dufour, Publ. Astron. Soc. Pacif. **107**, 896 (1995).
9. H. Nussbaumer and P. Storey, Astron. Astrophys. **70**, 37 (1978).
10. G. J. Ferland and G. A. Shields, Astrophys. J. **226**, 172 (1978).
11. L. H. Aller, *Physics of Thermal Gaseous Nebulae* (Reidel, Dodrecht, 1984).
12. R. E. S. Clegg, Mon. Not. R. Astron. Soc. **229**, 31 (1987).
13. H. Nussbaumer and P. J. Storey, Astron. Astrophys. **113**, 21 (1982).
14. V. V. Golovatyj, A. Sapar, T. Feklistova, and A. F. Kholtygin, Astron. Astrophys. Trans. **12**, 85 (1997).
15. P. Saizar, S. Starrfield, G. J. Ferland, R. M. Wagner, J. W. Truran, S. J. Kenyon, W. M. Sparks, R. E. Williams, and L. L. Stryker, Astrophys. J. **398**, 651 (1992).
16. J. Andrea, H. Drechsel, and S. Starrfield, Astron. Astrophys. **291**, 869 (1994).
17. V. P. Arkhipova, M. A. Burlak, and V. F. Esipov, Astron. Lett. **28**, 100 (2002).
18. T. N. Tarasova, Astron. Rep. **58**, 302 (2014).
19. T. N. Tarasova, Astron. Lett. **40**, 309 (2014).
20. T. N. Tarasova and A. Skopal, Astron. Lett. **42**, 10 (2016).
21. T. N. Tarasova, Astron. Rep. **57**, 95 (2013).
22. R. E. Williams, Astrophys. J. **426**, 279 (1994).

Translated by L. Yungel'son